



1 **Investigation of short-term effective radiative forcing of fire aerosols over North America**
2 **using nudged hindcast ensembles**

3 Yawen Liu^{1,2}, Kai Zhang², Yun Qian², Yuhang Wang³, Yufei Zou³, Yongjia Song³, Hui Wan²,
4 Xiaohong Liu⁴, and Xiu-Qun Yang¹

5

6 ¹ School of Atmospheric Sciences, Nanjing University, Nanjing, China

7 ² Pacific Northwest National Laboratory, Richland, Washington, USA

8 ³ School of Earth and Atmospheric Sciences, Georgia Institute of Technology, Atlanta, Georgia,
9 USA

10 ⁴ Department of Atmospheric Science, University of Wyoming, Laramie, Wyoming, USA

11

12

13 Corresponding to: Yun Qian [Yun.Qian@pnnl.gov]

14

15

16

17

18



19 **Abstract**

20 Aerosols from fire emissions can potentially have large impact on clouds and radiation. However,
21 fire aerosol sources are often intermittent and their effect on weather and climate is difficult to
22 quantify. Here we investigated the short-term effective radiative forcing of fire aerosols using the
23 global aerosol-climate model Community Atmosphere Model Version 5 (CAM5). Different from
24 previous studies, we used nudged hindcast ensembles to quantify the forcing uncertainty due to
25 the chaotic response to small perturbations in the atmosphere state. Daily mean emissions from
26 three fire inventories were used to consider the uncertainty in emission strength and injection
27 heights. The simulated aerosol optical depth (AOD) and mass concentrations were evaluated
28 against in-situ measurements and re-analysis data. Overall, the results show the model has
29 reasonably good predicting skills. Short (10-day) nudged ensemble simulations were then
30 performed with and without fire emissions to estimate the effective radiative forcing. Results
31 show fire aerosols have large effects on both liquid and ice clouds over the two selected regions
32 in April 2009. For the 10-day average, we found a large ensemble spread of regional mean
33 shortwave cloud radiative effect over Southern Mexico (15.6%) and the Central U.S. (64.3%),
34 despite that the regional mean AOD time series are almost indistinguishable during the 10-day
35 period. Moreover, the ensemble spread is much larger when using daily averages instead of 10-
36 day averages. For the case investigated here, a minimum of 9 ensemble members is necessary to
37 get a reasonable estimate of the ensemble mean and spread of the forcing on individual days.
38 This demonstrates the importance of using a large ensemble of simulations to estimate the short-
39 term effective aerosol radiative forcing.

40

41



42 1. Introduction

43 Natural and human-induced fires play an important role in the Earth system. Aerosol and gas
44 emissions from biomass burning can change the atmospheric composition and potentially affect
45 the weather and climate. Over 30% of the global total emission of black carbon (BC) comes from
46 open burning of forests, grasslands and agricultural residues (Bond et al. 2013). For organic
47 aerosols, substantial increases of concentrations dominated by organic carbon enhancements are
48 observed in regions with biomass burning events (Zeng et al. 2011; Lin et al. 2013; Brito et al.
49 2014; Reddington et al. 2014). As a result, biomass burning emissions have a large impact on
50 the global and regional mean aerosol optical depth (Jacobson, 2014).

51 Through interactions with radiation and clouds, fire aerosols can significantly affect the long-
52 term Earth's energy budget. Previous studies have investigated the global and regional radiative
53 forcing of fire aerosols using long climatological simulations or satellite retrievals. For example,
54 Ward et al. (2012) investigated the radiative forcing of global fires in pre-industrial, present day,
55 and future periods. For the present-day condition, they estimated a direct aerosol effect (or
56 radiative forcing through aerosol–radiation interactions as defined in IPCC AR5, RFari; see
57 section 2.4) of $+0.1 \text{ W m}^{-2}$ and an indirect effect (radiative forcing through aerosol–cloud
58 interactions, RFaci) of -1.0 W m^{-2} . Using a newer model, Jiang et al. (2016) found similar RFari
59 but slightly smaller RFaci (-0.70 W m^{-2}). Sena et al. (2013) assessed the direct impact of
60 biomass burning aerosols over the Amazon basin using satellite data. Over the 10-year studied
61 period, the estimated radiative forcing is about -5.6 W m^{-2} .

62 On short timescales, fire aerosols have even larger radiative impacts. Observed maximum
63 daily direct aerosol radiative effects can reach -20 W m^{-2} at TOA locally in Amazonia during
64 biomass burning seasons (Sena et al., 2013). Very large direct effects of fire aerosols were



65 observed during extreme fire events over Central Russia (Tarasova et al. 2004; Chubarova et al.
66 2008; Chubarova et al. 2012). Instantaneous radiative effects of emitted aerosols reached -167
67 W m^{-2} and monthly mean radiative effects reached about -65 W m^{-2} in the 2010 Russia
68 wildfires (Chubarova et al. 2012). Using satellite data and a radiative transfer model, Kaufman et
69 al. (2005) found a radiative effect of -9.5 W m^{-2} due to smoke aerosol-induced cloud changes over
70 Southeast Atlantic for the 3 months studied. Smoke-derived cloud albedo effect on local
71 shortwave radiative forcing is estimated to be between -2 and -4 W m^{-2} in a day case study of
72 aircraft-measured indirect cloud effects (Zamora et al., 2016). Kolusu et al. (2015) investigated
73 direct radiative effect of biomass burning aerosols over tropical Southern America. By
74 quantifying results from the first and second day of 2-day single-member forecasts in September
75 2012, they found the modeled biomass burning aerosols reduced all-sky net radiation by 8
76 W m^{-2} at TOA and 15 W m^{-2} at surface.

77 Previous modeling studies on the short-term fire aerosol effects mainly focused on aerosol
78 direct effects (e.g., Keil and Haywood, 2003; Chen et al., 2014; Kolusu et al., 2015), and only a
79 couple of studies investigated the indirect effects of fire aerosols (Lu and Sokolik, 2013). In
80 addition, to estimate the aerosol indirect effect, long simulations (multi-years, >5 years
81 preferred) are often needed to remove the noise, because aerosol life cycle and cloud properties
82 are affected by strong natural variability on different timescales (Bony et al. 2006; Kooperman et
83 al. 2012). To solve the problem, alternative methods have been proposed to help extract signals
84 with shorter simulations. For example, nudging (also called Newton relaxation method) can help
85 reduce uncertainties associated with natural variability by constraining certain meteorological
86 fields towards prescribed conditions. A robust estimate of global anthropogenic aerosol indirect
87 effects can be obtained on substantially shorter timescales (1-2 years) by implementing nudging



88 to constrain simulations with pre-industrial and present-day aerosol emissions toward identical
89 circulation and meteorology (Kooperman et al. 2012). When nudged towards re-analysis data,
90 Zhang et al. (2014) found constraining only the horizontal winds is a preferred strategy to
91 estimate the aerosol indirect effect since it provides well-constrained meteorology without
92 strongly perturbing the model's mean climate state. Another example is the use of representative
93 ensembles of short simulations to replace a typical long integration. Wan et al. (2014) explored
94 the feasibility of this method and showed that 3-day ensembles of 20 to 50 members are able to
95 reveal the main signals revealed by traditional 5-year simulations.

96 In this study, we performed month-long and 10-day nudged CAM5 simulations to investigate
97 the effects of fire aerosols on radiation and cloud processes on short time scales (less than two
98 weeks). Horizontal winds were nudged towards reanalysis to constrain the large-scale circulation
99 and to allow for more accurate model evaluations against observations. We also used daily mean
100 emissions from three fire inventories to consider the uncertainty in emission strength and
101 injection heights. Even for short simulations, small perturbations of meteorological states might
102 have large impact on the local aerosol and cloud properties, thus bring uncertainty to the aerosol
103 forcing estimate. Therefore, in our simulations, we also employed very weak temperature
104 nudging in combination with ensembles to quantify the uncertainty.

105 The rest of the paper is organized as follows. Sect. 2 describes the model and data used in this
106 study. It also introduces how the ensembles are generated in the short nudged simulations and
107 explains how the fire aerosol forcing is estimated. Results and discussions are presented in Sect.
108 3 and conclusions are summarized in Sect. 4.

109 **2. Model, Method and Data**



110 2.1 Model description

111 In this study, we used the Community Atmosphere Model (CAM) version 5.3 with the finite
112 volume dynamical core at 1.9° (latitude) \times 2.5° (longitude) horizontal resolution with 30 vertical
113 layers. The aerosol life cycle is represented by using the modal aerosol module MAM3 (Liu et
114 al., 2012). CAM5 links the simulated aerosol fields with cloud and radiation through interactions
115 of the aerosol module with the cloud microphysics and radiative transfer parameterizations. The
116 two-moment bulk cloud microphysics scheme from Morrison and Gettelman (2008) is used to
117 track mass mixing ratios and number concentrations of cloud droplets and ice crystals in
118 stratiform clouds. Representation of shallow convection is based on the work of Park and
119 Bretherton (2009). The deep convection parameterization was developed by Zhang and
120 McFarlane (1995) and later revised by Richter and Rasch (2008) and Neale et al. (2008).
121 Longwave and shortwave radiative transfer are calculated with the Rapid Radiative Transfer
122 Model for GCMs (RRTMG, Malwer et al. 1997; Iacono et al. 2008).

123 2.2 Fire Emission Inventories

124 Three fire emission inventories were used in this study. Two of them are widely used bottom-
125 up inventories— Global Fire Emissions Database version 3.1 (GFED v3.1, van der Werf et al.,
126 2010; https://daac.ornl.gov/cgi-bin/dsviewer.pl?ds_id=1191) and GFED v4.1s (Giglio et al.
127 2013; Randerson et al. 2012;
128 https://daac.ornl.gov/VEGETATION/guides/fire_emissions_v4.html). Another one is a top-down
129 emission inventory—Quick Fire Emissions Dataset version 2.4 (QFED v2.4). GFED v3.1 and
130 GFED v4.1s provide global monthly emissions at $0.25^\circ \times 0.25^\circ$ degree spatial resolution from 1997
131 through the present. Daily emission data are obtained by disaggregating monthly emissions



132 based on daily temporal variability in fire emissions derived from MODIS measurements of
133 active fires (Mu et al. 2011). The more recent version GFED v4.1s improves by including small
134 fires based on active fire detections outside the burned area maps (Randerson et al., 2012).
135 QFED v2.4 estimates global fire emissions using the Moderate Resolution Imaging
136 Spectroradiometer (MODIS) measurements of fire radiative power and generates daily products
137 at 0.1×0.1 degree resolution.

138 To drive CAM5 simulations, fire emission data were regridded to the model resolution and
139 distributed vertically. For the GFED v3.1 and QFED v2.4 emission data we adopted the same
140 injection heights (from surface to 6 km) as used in the standard CAM5 model. While for
141 GFEDv4.1s, in this study the injection heights were estimated using a fire plume model and
142 scaled to the 6-hourly interval.

143 The fire emission inventories were first analyzed to select appropriate time periods and
144 regions for our study before being used to drive model simulations. Fig.1 shows the multi-year
145 mean biomass burning emissions from GFED v4.1 over North America. The emission manifests
146 significant seasonality with large dry matter consumption during March to April and June to
147 September. The summer and autumn burning covers Pacific Northwest and part of Canada and is
148 mainly associated with forest fires, while the spring burning occurs in more densely populated
149 regions like Mexico and central and eastern United States with a large contribution of
150 agricultural fires in croplands (Korontzi et al., 2006; Magi et al., 2012). Similar features are also
151 captured in GFED v3.1 and QFED v2.4 with differences in the magnitude. We chose to analyze
152 the simulated fire aerosol effect in April, the peak month of spring burning, when there are
153 extreme fire activities over Mexico (10 N to 25N, 100W to 80W) and occasionally large fires in
154 the Central U.S. (35 N to 45N, 100W to 85W). For the U.S., extended fire period is rare, making



155 it necessary to perform short-term evaluation. Fire aerosols formed from these two regions are
156 often transported to the Eastern and Southeastern U.S., where they mix with aerosols from
157 anthropogenic sources and potentially have significant impact on clouds and radiation over these
158 areas. Time series of regional mean fire emissions in April during 2003-2014 shows that
159 relatively large fires occur in both regions in 2009 (Fig.S1). Values of fire emissions in 2009 are
160 larger than the multi-year April mean by a factor of 1.9 in the Central U.S. and 1.5 in Southern
161 Mexico. Thus, in the following model simulations, we focused on analyzing the aerosol
162 properties and radiative effects over the two selected regions (denoted by the red boxes in Fig.1)
163 in April 2009.

164 Fire emitted BC from different emission inventories in April 2009 is shown in Fig.2. Although
165 GFED v4.1s includes the contributions of small fires (Randerson et al., 2012), the emitted BC in
166 GFED v4.1 shows no substantial increase compared to GFED v3.1 during the selected period.
167 Only an increase by 1.75 is seen over Southern Mexico. In the Central U.S., the BC emission is
168 even slightly weaker in GFED v4.1. QFED v2.4 shows a much larger BC emission than the
169 GFED inventories. Values of emitted BC in QFED v2.4 are larger than those in GFED v4.1s by a
170 factor of 9.7 in the Central U.S. and a factor of 2.7 in Southern Mexico.

171 **2.3 Simulations**

172 Two groups of simulations were conducted (Table1) using the same greenhouse gas
173 concentrations, sea surface conditions and anthropogenic emissions of aerosols and precursors.
174 Each group includes four simulations, performed either without fire emission or with daily fire
175 emissions from one of the three fire emission inventories introduced in section 2.2. The emitted
176 species include BC, OC, and SO₂. Horizontal winds were nudged to 6-hourly ERA-Interim
177 reanalysis (Dee et al., 2011) as described in Zhang et al. (2014) in both groups.



178 Simulations in Group A are month-long single-member nudged simulations. These
179 simulations were performed to provide longer time series for model evaluation and generate
180 initial condition files for simulations in Group B. They started from January 1, 2009 and were
181 integrated for four months with 3-month spin-up. Initial condition files were generated on April
182 1 at 00 UTC for simulations in group B.

183 Simulations in group B are 10-day ensemble simulations. Unlike the traditional way of
184 perturbing initial conditions, in this study we constructed the ensembles by implementing a very
185 weak temperature nudging and perturbing the nudging time scale. This is because under the
186 influence of horizontal-wind nudging, ensemble differences generated by perturbing initial
187 conditions would fade away during the integration. In contrast, our method can consider the
188 influence of small temperature perturbations during the entire simulation period, as nudging is
189 applied at every time step. On the other hand, the large-scale circulation patterns simulated in the
190 different ensemble members are very similar (not shown), so the noises caused by the chaotic
191 system can be constrained and the effective fire aerosol forcing signal can be easily identified.

192 Each ensemble in group B includes 10 members. The only difference between the members is
193 the relaxation time scale of temperature, which varies from 10 to 11 days at an interval of 0.1
194 day. All simulations started on April 1, 2009 and were integrated for 10 days. For each
195 simulation (e.g. E_QF), the initial condition was generated by combining the meteorological
196 fields from initial condition outputs in the S_NF simulation with aerosol and precursor
197 concentrations from initial condition outputs in the single-member simulation forced by the
198 corresponding fire emission (S_QF).

199 **2.4 Calculation of fire aerosol RF**



200 The IPCC AR5 report provides a more useful characterization of aerosol forcing by allowing for
201 rapid tropospheric adjustments (Boucher et al., 2013) compared to the original definition of
202 aerosol forcing. It quantifies aerosol radiative effects in terms of Effective Radiative Forcing
203 from aerosol-radiation interactions (ERF_{ari}) and Effective Radiative Forcing from aerosol-cloud
204 interactions (ERF_{aci}). ERF_{ari} refers to the combined effect of instantaneous radiative forcing
205 from direct scattering and absorption of sunlight (aerosol direct effect) and related subsequent
206 rapid adjustments of atmospheric state variables and cloudiness (aerosol semi-direct effect).
207 ERF_{aci} refers to the indirect forcing resulting from aerosol induced changes in cloud albedo
208 (cloud albedo effect) and subsequent changes in cloud lifetime as rapid adjustments (second
209 aerosol indirect effect) via microphysical interactions.

210 To allow for a straightforward comparison with previous studies in the literature, we followed
211 the IPCC concept of including rapid adjustments (effective aerosol radiative forcing), but
212 continued to decompose the aerosol effect in the conventional terms as aerosol direct radiative
213 effect (DRE), aerosol cloud radiative effect (CRE) and surface albedo effect. Note that as
214 nudging timescale determines the degree to which model physics are constrained (Kooperman et
215 al., 2012), the use of a 6-hour relaxation time scale for horizontal wind nudging means only very
216 fast adjustments are considered in the simulations.

217 Similar to Jiang et al. (2016), our calculations of fire aerosol DRE, CRE and surface albedo
218 effect are based on the work of Ghan et al. (2012) and Ghan (2013). They were calculated as the
219 radiative flux differences between simulations with and without fire emissions (denoted by Δ). In
220 each simulation, aerosol (direct) forcing was defined as the difference between all-sky and clean-
221 sky TOA radiative fluxes ($F - F_{\text{clean}}$). Aerosol induced cloud forcing change was defined as the
222 difference between all-sky and clear sky TOA radiative fluxes under clean-sky



223 conditions ($F_{\text{clean}} - F_{\text{clean,clear}}$). The rest were related to surface albedo forcing ($F_{\text{clean,clear}}$).
224 Thus fire aerosol DRE, CRE, and surface albedo effect were expressed as $\Delta(F - F_{\text{clean}})$,
225 $\Delta(F_{\text{clean}} - F_{\text{clean,clear}})$, and $\Delta F_{\text{clean,clear}}$, respectively. More details about the method can be
226 found in section 2 of Ghan (2013). CRE includes contributions of both aerosol indirect effect and
227 aerosol semi-direct effect but was analyzed as a single term (i.e., the sum).

228 2.5 Observational Data

229 In this study, we used two sets of AOD reanalysis and the AERONET data (Holben et al.
230 1998) to evaluate the modeled AOD. The two AOD reanalysis datasets are the Naval Research
231 Laboratory (NRL) reanalysis (Rubin et al. 2015) and the Monitoring Atmospheric Composition
232 and Climate (MACC) reanalysis (Eskes et al. 2015). Both are generated by assimilating AOD
233 retrievals from MODIS (Zhang et al., 2008; Benedetti et al., 2009) with forecast fields. The NRL
234 reanalysis provides 6-hourly AOD at 1°horizontal resolution. The MACC dataset provides 3-
235 hourly AOD at 1.125°horizontal resolution. Daily averages in April, 2009 were used for model
236 evaluation in this study. AERONET retrievals of AOD from April 1 to April 30 in 2009 were
237 used for model evaluation. Two sites are available in the selected regions: Cart Site (36°N,
238 97°W) and Mexico City (19°N, 99°W). LEV 2.0 cloud-screened all points AOD at 500 nm and
239 675 nm was used to generate hourly AOD at 550nm.

240 In addition, the simulated BC and primary organic matter (POM) concentrations were
241 compared with observations from the Interagency Monitoring of Protected Visual Environments
242 (IMPROVE) (Malm et al. 2004). IMPROVE aerosol data are only available over the Central U.S.
243 A total of fifteen sites were selected and marked in Fig 2, which include the sites west of 94°W
244 near the source region (asterisks) and sites east of 94°W in the downwind region (dots).



245 Observed organic carbon concentrations were multiplied by 1.4 for comparison with simulated
246 POM. Detailed descriptions about the data and sites are available at
247 <http://vista.cira.colostate.edu/improve/>. The IMPROVE network collect 24-hour aerosol data on
248 every third day. Daily averages during April, 2009 are compared on IMPROVE observation days
249 only.

250 3. Results

251 In this part, the model performance is first evaluated based on the simulations in group A.
252 Next, we present the simulated short-term effective fire aerosol forcing on 10-day and daily
253 timescales based on the results from group B simulations. We will demonstrate the importance of
254 using ensemble simulations in estimating the short-term aerosol effective forcing and give a
255 quantitative estimate of how many ensemble members are needed for the case selected in this
256 study.

257 3.1 Model Evaluation

258 Model simulated AOD are evaluated against the NRL and MACC reanalysis data (Fig. 3).
259 The simulated temporal variation of regional mean AOD over the central U.S. is consistent with
260 that in the reanalysis, but the magnitudes of simulated AOD are lower (Fig. 3). A better
261 agreement is found between the model and the NRL data, despite the horizontal winds in the
262 simulation are nudged towards a reanalysis that is very similar to the data used to derive MACC.
263 Temporal correlation coefficients (TCC) between the modeled AOD and the NRL reanalysis are
264 0.87 and 0.82 for S_QF and S_GF4 simulations, respectively, but are lower (0.67 and 0.78)
265 between the modeled AOD and the MACC reanalysis. The corresponding root mean square



266 errors rise from 0.13 (S_QF) and 0.1 (S_GF4) to 0.23 and 0.21. Generally, AOD is
267 underestimated by a factor of 2-4 in all simulations compared to the reanalysis, especially in
268 simulations with GFED emissions. Previous studies have suggested the need to scale up GFED
269 emissions by a factor of 1-3 to match the observed AOD (Tosca et al., 2013). This is consistent
270 with the large negative bias in the simulation S_GF3 and S_GF4. Simulated AOD in these two
271 simulations are almost indistinguishable due to the small difference in the total fire emission in
272 the region.

273 Over Mexico, different simulations produce similar temporal variations in AOD, but the
274 magnitude is smaller in the GFED simulations. Large discrepancies are found between model
275 results and reanalysis data during Apr. 17-20. An increase of AOD is captured by both reanalysis
276 datasets, while model results display a decrease of AOD compared to earlier days in the
277 simulation period. Note that the two sets of reanalysis data also have some differences
278 occasionally. For example, during Apr. 10-12, NRL data displays an increase of AOD, while
279 MACC data show the opposite. These discrepancies may partly result from the large internal
280 variability in this tropical region, where the simulated atmosphere state and its influence on
281 aerosol transport are more likely to disagree between the model and the reanalysis. Generally
282 speaking, the model forced with different fire emissions is capable of capturing daily variation of
283 AOD in both regions, especially during Apr. 1-10. This period was selected for further
284 investigation of the short-term fire aerosol effect.

285 Model simulated AOD are also evaluated against AERONET retrievals (Fig. 4). At Cart Site
286 (36°N, 97°W), with the QFED emission (S_QF) the model performs well in simulating both the
287 temporal variation (TCC=0.62) and magnitude of AOD. Simulations with GFED emissions also
288 reproduce the temporal evolution well (TCC = 0.58 for S_GF3 and 0.55 for S_GF4), but with



289 significantly low bias (mean bias by a factor of 2). The simulated difference in AOD magnitude
290 is similar to that found by Zhang et al. (2014) over the northern sub-Saharan African. Using the
291 QFEDv2.4 fire emission, the simulated regional mean AOD is a factor of 1.5 higher than that
292 using the GFEDv3.1 emission in their study. Relatively good performance of S_QF is also seen
293 over Mexico. The simulated time evolution agrees well with AERONET retrievals except for
294 small discrepancies (e.g. during Apr.17 -19). A better agreement with the AERONET retrievals
295 is found for the NRL data than MACC reanalysis at both sites. Consistent with the evaluation
296 using reanalysis, the simulated temporal evolution of AOD during Apr. 1-10 agrees well with
297 both reanalysis data and AERONET retrievals in selected regions. This gives us further
298 confidence in choosing this period for further investigation.

299 The model is further evaluated against the IMPROVE data for BC and POM mass
300 concentrations (Fig. 5). In the downwind region, the simulated mass concentrations in simulation
301 S_QF lie within a factor of 2 of the observed values at most sites. However, the magnitude is
302 generally underestimated in simulations with the GFED emissions (S_GF3 and S_GF4),
303 especially in S_GF3. BC and POM concentrations in the downwind regions are affected by
304 transport of aerosols from Southern Mexico (Fig. S3). A larger amount of fire emission in
305 Southern Mexico would result in a higher BC (POM) concentration in the downwind region.
306 This explains the slightly higher concentrations in the simulation S_GF4 than S_GF3, as BC and
307 POM emissions over Southern Mexico are higher in GFED v4.1 due to the inclusion of small
308 fires (Randerson et al., 2012). The good agreement between S_QF and observations suggests that
309 the QFED data have a reasonable total emission rate. However, in the source region, the
310 simulation S_QF displays large positive bias with a large majority of the values fall out of the a-
311 factor-of-2 band. Given the reasonable total emission rate in QFED and a good agreement of



312 AOD with AERONET retrievals at Cart Site, this might result from the discrepancies in the
313 vertical distribution of the fire emissions. Fire-emitted BC and POM in simulations S_QF and
314 S_GF3 reach maximum values in the lowest level and decrease sharply to the next level, while
315 low-level fire emissions in S_GF4 distribute in a more uniform way (Fig. S4). As the sampling
316 was done on the lowest model level at most sites to compare with the IMPROVE data, this
317 explains the strong overestimation in S_QF. Although the same impact from vertical distribution
318 of fire emission also appears in simulation S_GF3, it is partly offset by its negative bias in the
319 total emission rate.

320 **3.2 10-day Mean Results**

321 Given the good model performance during April 1-10, we proceed to analyze the short-term
322 effects of fire aerosols during this period with nudged ensemble simulations. We define “fire
323 AOD” as the AOD difference between the simulations with and without fire emissions.

324 **3.2.1 Fire Aerosol Distribution**

325 Fig. 6 shows the spatial distributions of 10-day average ensemble mean fire AOD. For
326 reference, the total AOD in the simulation without fire emissions is shown in Fig. S2. During the
327 period, regional mean AOD increases by 6.4% (E_GF3), 6.4% (E_GF4) and 70.2% (E_QF) in
328 the central U.S. and 10.4% (E_GF3), 13.3% (E_GF4), and 49.6% (E_QF) in Southern Mexico
329 when fire emissions are included. In E_QF, high fire AOD covers almost the entire selected
330 region and extends further north. Maximum values of fire AOD stay above 0.2 around the
331 Yucatan Peninsula. Over the Central U.S, significant fire AOD ranging between 0.04 and 0.1
332 appears in the southwest part of the selected region. Apart from the significant AOD difference
333 in selected regions, large fire AOD also appears near the eastern coast as a result of local fire



334 emission and the eastward transport of fire aerosols from both regions. Overall, the modeled fire
335 AOD is much smaller in simulations with GFED emissions.

336 **3.2.2 Fire Aerosol Radiative Effect**

337 As described in Sect. 2.4, fire aerosol radiative effect can be decomposed into three items
338 including fire aerosol DRE, fire aerosol CRE and fire aerosol surface albedo effect. Fig.7 shows
339 the spatial distributions of shortwave direct effect (SDRE) and shortwave cloud radiative effect
340 (SCRE). They are major contributors to the total fire aerosol forcing in the selected regions. For
341 reference, total aerosol forcing and total shortwave cloud forcing in the simulation without fire
342 emissions are shown in Fig. S2. The spatial distribution of SDRE and SCRE are similar for the
343 three cases, but with different magnitudes and statistical significant regions for simulations with
344 QFED and GFED fire emissions. In the Central U.S., fire aerosol SDRE is negligible in GFED
345 forced simulations due to small fire AOD. Although the fire AOD is larger in simulation E_QF,
346 the compensation between warming effect of fire BC and cooling effect of fire POM still results
347 a weak forcing of about -0.1W m^{-2} . Over southern Mexico, all simulations produce significant
348 cooling by fire aerosol SCRE with maximum values three times as large as those of
349 corresponding SDRE. For both SDRE and SCRE, the largest fire aerosol effects appear in the
350 E_QF simulation while the E_GF3 yields the weakest forcing, which is consistent with the
351 modeled fire AOD in these simulations.

352 In the following analysis, we will focus on the results from the E_QF simulation. Both SDRE
353 and SCRE spread outside the two selected regions and extend eastward reaching coast regions. A
354 stronger fire aerosol effect is seen in the Southern Mexico region. Strong SDRE appears over the
355 Yucatan Peninsula where fire AOD peaks (Fig. 6). Regional mean 10-day average of SDRE and
356 SCRE reach -1.66W m^{-2} and -3.02W m^{-2} respectively. In the central U.S, despite moderate fire



357 aerosol SDRE, SCRE near fire source region is weaker than -4 W m^{-2} , which is comparable to
358 that in the extended regions.

359 Given the largely insignificant change in cloud fraction (Fig. 8), fire aerosol SCRE in both
360 regions are mainly induced by changes in liquid water path (LWP) and droplet number
361 concentrations (CDNC). Changes in ice water path (IWP) and ice crystal number concentration
362 (ICNC) can also significantly affect SCRE, but with an opposite sign and mostly in the central
363 U.S. Fire aerosol SCRE in the central U.S is associated with significant increases in both
364 column-integrated droplet number concentration (smaller droplet effective radius) and LWP,
365 indicating important contributions of both the aerosol first and second indirect effects. Increased
366 CDNC enhances cloud albedo by decreasing droplet sizes (Twomey, 1977) and allows more
367 liquid water to accumulate by decreasing precipitation efficiency (Albrecht, 1989; Ghan et al.,
368 2012). Note that although LWP and CDNC over southern Mexico change in a smaller magnitude
369 than those in central U.S., fire aerosol SCRE is stronger over Southern Mexico. This is mainly
370 due to the reductions in IWP and ICNC over the Central U.S. These changes, which possibly
371 caused by fire aerosol-induced changes in the circulation (Ten Hoeve et al, 2012), lead to a
372 positive SCRE that partly offsets the negative SCRE caused by changes in warm clouds. In the
373 northeast of the extended coastal regions, a more significant change of LWP comparable to that
374 in the central U.S appears, while a more significant change of CDNC comparable to that in
375 Southern Mexico occurs in the southwest. The combined effect leads to the total fire aerosol
376 effect in the extended regions.

377 The ensemble method provides another effective way to distinguish fire aerosol radiative
378 effect by comparing the radiative forcing distribution of ensemble members between simulations
379 with and without fire emission. A significant difference in the distribution of total aerosol (cloud)



380 forcing indicates a significant fire aerosol direct (cloud) effect. As shown in Fig. 9, a shift
381 towards stronger magnitude occurs to the total aerosol forcing when fire aerosols are considered.
382 Simulation E_QF has a larger percentage of grid cells with SDRE below -4.2 W m^{-2} , while more
383 grid cells exceed -4.2 W m^{-2} in E_NF, which indicates a significant negative fire aerosol direct
384 effect. Same shift also appears to the total cloud forcing with more grid cells having cloud
385 forcing below -30 W m^{-2} in the simulation E_QF. Regional mean total aerosol and cloud forcing
386 in southern Mexico become more negative (-0.86 and -3.0 W m^{-2}) with fire aerosols.

387 Fig. 10 illustrates ensemble behavior of 10-day average regional mean total aerosol and cloud
388 forcing from all simulations as well as resulted fire aerosol SDRE and SCRE. The GFED forced
389 simulations not only resemble in ensemble mean, but also have small difference in ensemble
390 member distribution. Although members in the E_QF simulation capture stronger aerosol
391 forcing, thus stronger fire aerosol SDRE than those in E_GF3 and E_GF4, the ensemble spread
392 (as indicated by the maximum and minimum values) in the three simulations is similar.
393 Moreover, the E_QF simulation yields a smaller spread of SCRF compared with the GFED
394 forced simulations despite a stronger ensemble mean SCRF. In each fire simulation, ensemble
395 mean fire aerosol SCRE has a much larger magnitude than SDRE. So is the corresponding
396 ensemble spread. Taking results from E_QF simulation as an example, ensemble spread of
397 SCRE reaches 0.47 W m^{-2} , accounting for 15.6% of the corresponding ensemble mean, while
398 ensemble spread of SDRE is 0.03 W m^{-2} accounting for 3.5% of the corresponding ensemble
399 mean.

400 3.3 Daily RF

401 The fire aerosol effect is also investigated for individual days. The spatial distributions of
402 SDRE and SCRE on April 7 are shown in Fig 11, when relatively high fire emissions appear in



403 both regions. Negative fire aerosol SDRE appears in the central U.S. biomass-burning region
404 indicating the dominant role of POM scattering. Fire aerosol SDRE over Southern Mexico shows
405 a contrast of warming effect in land region and cooling effect in adjacent ocean despite similar
406 aerosol loading in the two regions. However, they do have nearly equal clear-sky BC absorption
407 and POM scattering (Fig. 12). Difference in the low-level cloud distributions between two
408 regions leads to different signs of the simulated all-sky SDRE. Over land, when clouds appear
409 under elevated aerosol layers, more solar radiation is reflected back to space and this leads to
410 amplified BC absorption and more positive direct aerosol forcing (Keil and Haywood, 2003;
411 Zhang et al., 2016; Jiang et al., 2016). In contrast, neither absorption nor scattering changes
412 significantly from clear-sky to all-sky condition over adjacent areas over the ocean, since the
413 cloud fraction is small. Same enhanced absorption of above-cloud aerosols is also found over the
414 west Atlantic Ocean. Fire aerosols produce remarkable negative SCRE up to -16W m^{-2} over
415 Southern Mexico land in response to the increase in CDNC and LWP.

416 **3.4 Discussion about the Simulation Strategy**

417 Fig. 13 shows the daily variation of the regional mean total (direct) aerosol forcing and cloud
418 forcing. Both the ensemble mean and spread are investigated here. The total aerosol forcing
419 exhibits considerable diversity across ensemble members within each simulation, even though
420 the simulated AOD is nearly indistinguishable (Fig. 3). Taking results from simulation E_QF as
421 an example, maximum values of difference between members exceed 0.4 W m^{-2} for aerosol
422 forcing and 5 W m^{-2} for cloud forcing, which are approximate 10% of the corresponding
423 ensemble mean values. The large spread of total aerosol forcing and cloud forcing will lead to
424 uncertainties in the estimation of fire aerosol effect. This points out the importance of conducting
425 ensemble simulations in order to get a more comprehensive estimate of the daily fire aerosol



426 effect. The minimum ensemble size required for this case is investigated in terms of the
427 ensemble mean and spread estimate. Simulated ensemble mean fire aerosol SDRE remains
428 nearly unchanged regardless of the ensemble size (Fig. 14a). However, discrepancies in the
429 ensemble mean fire aerosol SCRE (Fig. 14b) are substantial when the number of ensemble
430 members is smaller than 8. The same is true for the ensemble spread of fire aerosol SCRE (Fig.
431 S5). Overall, the time evolution and magnitude of ensemble mean and spread tend to converge
432 when the number of ensemble members reaches about 9 for different days we investigated here.

433 Fire aerosol sources are often intermittent and height-dependent and there is a need to
434 estimate the short-term effective aerosol forcing. Although nudging helps to constrain large-scale
435 features, the simulated cloud properties (e.g. cloud fraction and LWP) and their response to
436 aerosol changes can still be sensitive to small perturbations in the atmospheric state. Therefore,
437 for investigating the short-term aerosol effect, a single simulation might not be sufficient to tell
438 whether the aerosol effect is significant. The use of ensembles provides an effective way to
439 estimate the uncertainty. Previous investigations of short-term fire aerosol effect are mainly
440 based on single-member simulations (Wu et al., 2011; Sena et al., 2013; Kolusu et al., 2015).
441 While this might be less a problem for SDRE, one should be more careful when investigating the
442 aerosol indirect effect and conduct ensemble simulations to see whether the estimated fire
443 aerosol effects are robust.

444 **4. Summary**

445 In this study, we investigated the short-term effect of fire aerosols on cloud and radiation
446 using CAM5 simulations. Month-long single-member simulations and 10-day ensemble
447 simulations were conducted in April 2009. In order to help extract signals on short time scales,



448 we used nudging to constrain horizontal winds in all simulations. Our investigation focused on
449 Southern Mexico where there were constant intensive fire activities and the Central U.S. with
450 occasionally large fires. Apart from the local effect, fire emissions from the two regions are
451 shown to affect downwind coastal regions through transport.

452 Modeled AOD and mass concentrations (BC and POM) were evaluated against observations.
453 In general, all simulations with fire emissions reproduce the observed temporal variation of daily
454 mean AOD well, although the simulated magnitude is smaller. The model performance is better
455 when QFEDv2.4 is used, which has larger fire emissions. Modeled regional mean AOD values in
456 simulations using two versions of GFED fire emission data are barely distinguishable, despite the
457 inclusion of small fires and changed injection heights in GFEDv4.1 used in this study. Both of
458 them simulate about a factor of 1.5 smaller AOD than that in the simulation using the QFED fire
459 emissions. At sites in the downwind region, the modeled BC and POM mass concentrations in
460 the simulation with QFEDv2.4 emission (S_QF) agree well with the IMPROVE data. In contrast,
461 simulations with the other two fire emission datasets (S_GF3 and S_GF4) have a low bias. The
462 simulated AOD in the source region in S_QF also agrees well with the AERONET data (Cart
463 Site). If there is no large compensating error in the model, QFEDv2.4 seems more reasonable in
464 terms of the total (vertically-integrated) emission rate. On the other hand, S_QF strongly
465 overestimates BC and POM concentrations in the source region. Considering that the source-
466 region AOD and the downwind surface mass concentrations are well simulated, the
467 overestimation suggests that the actual emission peak might appear at higher levels compared to
468 the height-dependent injection rates applied in the S_QF simulation.

469 Based on the evaluation, we chose the first 10 days as the simulation period and focused on
470 the simulation with QFEDv2.4 fire emission in our ensemble nudged simulations. In our method,



471 the nudged ensembles are generated by adding a very weak temperature nudging along with
472 horizontal-wind nudging and perturbing the nudging time scale of temperature gently. In this
473 way, small temperature perturbations are added to the simulation at each time step, while the
474 large-scale circulation features are very similar between individual members. We first
475 investigated the 10-day mean effective fire aerosol forcing. Decomposition of total aerosol
476 radiative forcing shows that fire aerosol effects in the two selected regions are dominated by the
477 shortwave cloud radiative effect SCRE. All fire simulations show similar spatial distribution of
478 SDRE and SCRE, but with different magnitudes and statistically significant regions. The
479 similarity in the spatial distribution is expected since the three emission datasets differ mainly in
480 the emission magnitude and not much in spatial distribution in the focused regions of this study.
481 Fire aerosol effects in simulations with GFED emissions (E_GF3 and E_GF4) are weaker than
482 that with QFEDv2.4 emission (E_QF) by a factor of 1.5 for SCRE and a factor of more than 4
483 for SDRE. Generally speaking, the difference in simulated AOD and fire aerosol indirect
484 radiative effects between simulations is smaller compared to the difference between fire
485 emissions, consistent with the findings in sub-Saharan African biomass-burning region (Zhang et
486 al. 2014).

487 Fire aerosols produce a negative direct effect of -0.1 W m^{-2} in the Central U.S. and -0.86
488 W m^{-2} in Southern Mexico in E_QF during the 10-day period. Within each region, negative fire
489 aerosol SDRE peaks where fire AOD reaches maximum. Unlike the limited area affected by
490 significant fire aerosol SDRE, fire aerosol SCRE from selected regions spreads eastward and
491 northward, affecting remote coastal regions. Maximum SCRE stays below -4 W m^{-2} in the
492 central U.S. and -10 W m^{-2} in Southern Mexico in response to significantly increased LWP and
493 CDNC. Decreases of IWP and ICNC also contribute to fire aerosol SCRE in the Central U.S. but



494 with an opposite sign. The offset effect of the positive forcing induced by changes in cloud ice
495 properties explains the smaller SCRE in the central U.S. despite the larger changes in cloud
496 droplet properties.

497 We also investigated fire aerosol effects on the daily time scale, where the variation in the
498 simulated fire aerosol effect can be large among the ensemble members. The large ensemble
499 spread of total aerosol and cloud forcing indicates large uncertainties in estimating daily fire
500 aerosol effects, despite similar AOD across ensemble members. Further investigations show that
501 the simulated ensemble mean and spread with less than 7 members differs considerably to those
502 with more members. A minimum of 9 members is necessary to achieve a steady estimate of the
503 magnitude and temporal variation of SCRE in this case. Our results suggest that for short-term
504 simulations of aerosol and cloud processes, even small perturbations might result in large
505 difference across members despite constrained large scale features. In order to obtain a robust
506 estimate of the effective fire aerosol forcing during a short period, it is important to conduct
507 ensemble simulations with sufficient ensemble members.

508

509 **Acknowledgments**

510 This study was supported by the U.S. Department of Energy (DOE)'s Office of Science as part
511 of the Regional and Global Climate Modeling Program (NSF-DOE-USDA EaSM2). The work
512 was also supported by the National Natural Science Foundation of China (NSFC) under Grants
513 No. 41621005 and 41330420, the National Key Basic Research Program (973 Program) of China
514 under Grant No. 2010CB428504, and the Jiangsu Collaborative Innovation Center of Climate.
515 The Pacific Northwest National Laboratory (PNNL) is operated for DOE by Battelle Memorial



516 Institute under contract DE-AC05-76RL01830. Computations were performed using resources of
517 the National Energy Research Scientific Computing Center (NERSC) at Lawrence Berkeley
518 National Laboratory and PNNL Institutional Computing. All model results are available from the
519 corresponding author upon request.



520 **References:**

- 521 Albrecht, B. A.: Aerosols, cloud microphysics, and fractional cloudiness, *Science*, 245, 1227-
522 1231, 1989.
- 523 Benedetti, A., Morcrette, J. J., Boucher, O., Dethof, A., Engelen, R., Fisher, M., Flentje, H.,
524 Huneeus, N., Jones, L., and Kaiser, J.: Aerosol analysis and forecast in the European centre for
525 medium-range weather forecasts integrated forecast system: 2. Data assimilation, *Journal of*
526 *Geophysical Research: Atmospheres*, 114, 2009.
- 527 Bond, T. C., Doherty, S. J., Fahey, D., Forster, P., Berntsen, T., DeAngelo, B., Flanner, M.,
528 Ghan, S., Kärcher, B., and Koch, D.: Bounding the role of black carbon in the climate system: A
529 scientific assessment, *Journal of Geophysical Research: Atmospheres*, 118, 5380-5552, 2013.
- 530 Bony, S., Colman, R., Kattsov, V. M., Allan, R. P., Bretherton, C. S., Dufresne, J.-L., Hall, A.,
531 Hallegatte, S., Holland, M. M., and Ingram, W.: How well do we understand and evaluate
532 climate change feedback processes?, *Journal of Climate*, 19, 3445-3482, 2006.
- 533 Boucher, O., Randall, D., Artaxo, P., Bretherton, C., Feingold, G., Forster, P., Kerminen, V.-M.,
534 Kondo, Y., Liao, H., and Lohmann, U.: Clouds and aerosols, in: *Climate change 2013: the*
535 *physical science basis. Contribution of Working Group I to the Fifth Assessment Report of the*
536 *Intergovernmental Panel on Climate Change*, Cambridge University Press, 571-657, 2013.
- 537 Brito, J., Rizzo, L. V., Morgan, W. T., Coe, H., Johnson, B., Haywood, J., Longo, K., Freitas, S.,
538 Andreae, M. O., and Artaxo, P.: Ground-based aerosol characterization during the South
539 American Biomass Burning Analysis (SAMBBA) field experiment, *Atmospheric Chemistry and*
540 *Physics*, 14, 12069-12083, 2014.



- 541 Chen, D., Liu, Z., Schwartz, C. S., Lin, H.-C., Cetola, J. D., Gu, Y., and Xue, L.: The impact of
542 aerosol optical depth assimilation on aerosol forecasts and radiative effects during a wild fire
543 event over the United States, *Geoscientific Model Development*, 7, 2709-2715, 2014.
- 544 Chubarova, N., Nezval, Y., Sviridenkov, I., Smirnov, A., and Slutsker, I.: Smoke aerosol and its
545 radiative effects during extreme fire event over Central Russia in summer 2010, *Atmospheric*
546 *Measurement Techniques*, 5, 557-568, 2012.
- 547 Chubarova, N. Y., Prilepsky, N. G., Rublev, A. N., and Riebau, A. R.: A Mega-Fire event in
548 central Russia: fire weather, radiative, and optical properties of the atmosphere, and
549 consequences for subboreal forest plants, *Developments in environmental science*, 8, 247-264,
550 2008.
- 551 Dee, D., Uppala, S., Simmons, A., Berrisford, P., Poli, P., Kobayashi, S., Andrae, U., Balmaseda,
552 M., Balsamo, G., and Bauer, P.: The ERA-Interim reanalysis: Configuration and performance of
553 the data assimilation system, *Quarterly Journal of the royal meteorological society*, 137, 553-
554 597, 2011.
- 555 Eskes, H., Huijnen, V., Arola, A., Benedictow, A., Blechschmidt, A.-M., Botek, E., Boucher, O.,
556 Bouarar, I., Chabrillat, S., and Cuevas, E.: Validation of reactive gases and aerosols in the
557 MACC global analysis and forecast system, *Geoscientific model development*, 8, 3523-3543,
558 2015.
- 559 Ghan, S. J., Liu, X., Easter, R. C., Zaveri, R., Rasch, P. J., Yoon, J.-H., and Eaton, B.: Toward a
560 minimal representation of aerosols in climate models: Comparative decomposition of aerosol
561 direct, semidirect, and indirect radiative forcing, *Journal of Climate*, 25, 6461-6476, 2012.
- 562 Ghan, S. J.: Technical Note: Estimating aerosol effects on cloud radiative forcing, *Atmos. Chem.*
563 *Phys.*, 13, 9971-9974, doi:10.5194/acp-13-9971-2013, 2013.



564 Giglio, L., Randerson, J. T., and van der Werf, G. R. (2013), Analysis of daily, monthly, and
565 annual burned area using the fourth-generation global fire emissions database (GFED4) J.
566 Geophys. Res. Biogeosci., 118, 317–328, doi:10.1002/jgrg.20042.

567 Holben, B. N., Eck, T., Slutsker, I., Tanre, D., Buis, J., Setzer, A., Vermote, E., Reagan, J.,
568 Kaufman, Y., and Nakajima, T.: AERONET—A federated instrument network and data archive
569 for aerosol characterization, Remote sensing of environment, 66, 1-16, 1998.

570 Iacono, M. J., Delamere, J. S., Mlawer, E. J., Shephard, M. W., Clough, S. A., and Collins, W.
571 D.: Radiative forcing by long-lived greenhouse gases: Calculations with the AER radiative
572 transfer models, Journal of Geophysical Research: Atmospheres, 113, 2008.

573 Jacobson, M. Z.: Effects of biomass burning on climate, accounting for heat and moisture fluxes,
574 black and brown carbon, and cloud absorption effects, Journal of Geophysical Research:
575 Atmospheres, 119, 8980-9002, 2014.

576 Jiang, Y., Lu, Z., Liu, X., Qian, Y., Zhang, K., Wang, Y., and Yang, X.-Q.: Impacts of global
577 open-fire aerosols on direct radiative, cloud and surface-albedo effects simulated with CAM5,
578 Atmospheric Chemistry and Physics (Online), 16, 2016.

579 Kaufman, Y. J., Koren, I., Remer, L. A., Rosenfeld, D., and Rudich, Y.: The effect of smoke,
580 dust, and pollution aerosol on shallow cloud development over the Atlantic Ocean, Proceedings
581 of the National Academy of Sciences of the United States of America, 102, 11207-11212, 2005.

582 Keil, A., and Haywood, J. M.: Solar radiative forcing by biomass burning aerosol particles
583 during SAFARI 2000: A case study based on measured aerosol and cloud properties, Journal of
584 Geophysical Research: Atmospheres, 108, 2003.



- 585 Kolusu, S., Marsham, J., Mulcahy, J., Johnson, B., Dunning, C., Bush, M., and Spracklen, D.:
586 Impacts of Amazonia biomass burning aerosols assessed from short-range weather forecasts,
587 Atmospheric Chemistry and Physics, 15, 12251-12266, 2015.
- 588 Kooperman, G. J., Pritchard, M. S., Ghan, S. J., Wang, M., Somerville, R. C., and Russell, L. M.:
589 Constraining the influence of natural variability to improve estimates of global aerosol indirect
590 effects in a nudged version of the Community Atmosphere Model 5, Journal of Geophysical
591 Research: Atmospheres, 117, 2012.
- 592 Korontzi, S., McCarty, J., Loboda, T., Kumar, S., and Justice, C.: Global distribution of
593 agricultural fires in croplands from 3 years of Moderate Resolution Imaging Spectroradiometer
594 (MODIS) data, Global Biogeochemical Cycles, 20, 2006.
- 595 Lin, N.-H., Tsay, S.-C., Maring, H. B., Yen, M.-C., Sheu, G.-R., Wang, S.-H., Chi, K. H.,
596 Chuang, M.-T., Ou-Yang, C.-F., and Fu, J. S.: An overview of regional experiments on biomass
597 burning aerosols and related pollutants in Southeast Asia: From BASE-ASIA and the Dongsha
598 Experiment to 7-SEAS, Atmospheric Environment, 78, 1-19, 2013.
- 599 Liu, X., Easter, R. C., Ghan, S. J., Zaveri, R., Rasch, P., Shi, X., Lamarque, J.-F., Gettelman, A.,
600 Morrison, H., and Vitt, F.: Toward a minimal representation of aerosols in climate models:
601 Description and evaluation in the Community Atmosphere Model CAM5, Geoscientific Model
602 Development, 5, 709, 2012. Jiang, Y.: Impacts of global open-fire aerosols on direct radiative,
603 cloud and surface-albedo effects simulated with CAM5, Atmos. Chem. Phys., 1680, 7324, 2016.
- 604 Lu, Z., and Sokolik, I. N.: The effect of smoke emission amount on changes in cloud properties
605 and precipitation: A case study of Canadian boreal wildfires of 2007, Journal of Geophysical
606 Research: Atmospheres, 118, 2013.



- 607 Magi, B., Rabin, S., Shevliakova, E., and Pacala, S.: Separating agricultural and non-agricultural
608 fire seasonality at regional scales, *Biogeosciences*, 9, 3003, 2012.
- 609 Malm, W. C., Schichtel, B. A., Pitchford, M. L., Ashbaugh, L. L., and Eldred, R. A.: Spatial and
610 monthly trends in speciated fine particle concentration in the United States, *Journal of*
611 *Geophysical Research: Atmospheres*, 109, 2004.
- 612 Mlawer, E. J., Taubman, S. J., Brown, P. D., Iacono, M. J., and Clough, S. A.: Radiative transfer
613 for inhomogeneous atmospheres: RRTM, a validated correlated-k model for the longwave,
614 *Journal of Geophysical Research: Atmospheres*, 102, 16663-16682, 1997.
- 615 Morrison, H., and Gettelman, A.: A new two-moment bulk stratiform cloud microphysics
616 scheme in the Community Atmosphere Model, version 3 (CAM3). Part I: Description and
617 numerical tests, *Journal of Climate*, 21, 3642-3659, 2008.
- 618 Mu, M., Randerson, J., van der Werf, G., Giglio, L., Kasibhatla, P., Morton, D., Collatz, G.,
619 DeFries, R., Hyer, E., and Prins, E.: Daily and hourly variability in global fire emissions and
620 consequences for atmospheric model predictions of carbon monoxide, 2011.
- 621 Neale, R. B., Richter, J. H., and Jochum, M.: The impact of convection on ENSO: From a
622 delayed oscillator to a series of events, *Journal of Climate*, 21, 5904-5924, 2008.
- 623 Park, S., and Bretherton, C. S.: The University of Washington shallow convection and moist
624 turbulence schemes and their impact on climate simulations with the Community Atmosphere
625 Model, *Journal of Climate*, 22, 3449-3469, 2009.
- 626 Randerson, J., Chen, Y., Werf, G., Rogers, B., and Morton, D.: Global burned area and biomass
627 burning emissions from small fires, *Journal of Geophysical Research: Biogeosciences*, 117,
628 2012.



- 629 Reddington, C., Yoshioka, M., Balasubramanian, R., Ridley, D., Toh, Y., Arnold, S., and
630 Spracklen, D.: Contribution of vegetation and peat fires to particulate air pollution in Southeast
631 Asia, *Environmental Research Letters*, 9, 094006, 2014.
- 632 Richter, J. H., and Rasch, P. J.: Effects of convective momentum transport on the atmospheric
633 circulation in the Community Atmosphere Model, version 3, *Journal of Climate*, 21, 1487-1499,
634 2008.
- 635 Rubin, J. I., Reid, J. S., Hansen, J. A., Anderson, J. L., Hoar, T. J., Reynolds, C. A., Sessions, W.
636 R., and Westphal, D. L.: Development of the Ensemble Navy Aerosol Analysis Prediction
637 System (ENAAPS) and its application of the Data Assimilation Research Testbed (DART) in
638 support of aerosol forecasting, *Atmospheric Chemistry and Physics*, 16, 3927, 2016.
- 639 Sena, E., Artaxo, P., and Correia, A.: Spatial variability of the direct radiative forcing of biomass
640 burning aerosols and the effects of land use change in Amazonia, *Atmospheric Chemistry and*
641 *Physics*, 13, 1261-1275, 2013.
- 642 Stier, P., Schutgens, N., Bellouin, N., Bian, H., Boucher, O., Chin, M., Ghan, S., Huneeus, N.,
643 Kinne, S., and Lin, G.: Host model uncertainties in aerosol radiative forcing estimates: results
644 from the AeroCom Prescribed intercomparison study, *Atmospheric Chemistry and Physics*, 13,
645 3245-3270, 2013.
- 646 Tarasova, T., Gorchakova, I., Sviridenkov, M., Anikin, P., and Romashova, E.: Estimation of the
647 radiative forcing of smoke aerosol from radiation measurements at the Zvenigorod scientific
648 station in the summer of 2002, *Izvestiya Atmospheric and Oceanic Physics*, 40, 454-463, 2004.
- 649 Ten Hoeve, J. E., Jacobson, M. Z., and Remer, L. A.: Comparing results from a physical model
650 with satellite and in situ observations to determine whether biomass burning aerosols over the
651 Amazon brighten or burn off clouds, *Journal of Geophysical Research: Atmospheres*, 117, 2012.



- 652 Tosca, M., Randerson, J., and Zender, C.: Global impact of smoke aerosols from landscape fires
653 on climate and the Hadley circulation, *Atmospheric Chemistry and Physics*, 13, 5227-5241,
654 2013.
- 655 Twomey, S.: The influence of pollution on the shortwave albedo of clouds, *Journal of the*
656 *atmospheric sciences*, 34, 1149-1152, 1977.
- 657 van der Werf, G. R., Randerson, J. T., Giglio, L., Collatz, G. J., Mu, M., Kasibhatla, P. S.,
658 Morton, D. C., DeFries, R. S., Jin, Y., and van Leeuwen, T. T.: Global fire emissions and the
659 contribution of deforestation, savanna, forest, agricultural, and peat fires (1997–2009), *Atmos.*
660 *Chem. Phys.*, 10, 11707-11735, doi:10.5194/acp-10-11707-2010, 2010.
- 661 Ward, D., Kloster, S., Mahowald, N., Rogers, B., Randerson, J., and Hess, P.: The changing
662 radiative forcing of fires: global model estimates for past, present and future, *Atmospheric*
663 *Chemistry and Physics*, 12, 2012.
- 664 Wan, H., Rasch, P. J., Zhang, K., Qian, Y., Yan, H., and Zhao, C.: Short ensembles: an efficient
665 method for discerning climate-relevant sensitivities in atmospheric general circulation models,
666 *Geoscientific Model Development*, 7, 1961-1977, 2014.
- 667 Wu, L., Su, H., and Jiang, J. H.: Regional simulations of deep convection and biomass burning
668 over South America: 2. Biomass burning aerosol effects on clouds and precipitation, *Journal of*
669 *Geophysical Research: Atmospheres*, 116, 2011.
- 670 Zamora, L. M., Kahn, R., Cubison, M. J., Diskin, G., Jimenez, J., Kondo, Y., McFarquhar, G.,
671 Nenes, A., Thornhill, K., and Wisthaler, A.: Aircraft-measured indirect cloud effects from
672 biomass burning smoke in the Arctic and subarctic, *Atmospheric Chemistry and Physics*, 16,
673 715-738, 2016.



674 Zhang, F., Wang, J., Ichoku, C., Hyer, E. J., Yang, Z., Ge, C., Su, S., Zhang, X., Kondragunta,
675 S., and Kaiser, J. W.: Sensitivity of mesoscale modeling of smoke direct radiative effect to the
676 emission inventory: a case study in northern sub-Saharan African region, *Environmental*
677 *Research Letters*, 9, 075002, 2014.

678 Zhang, G. J., and McFarlane, N. A.: Sensitivity of climate simulations to the parameterization of
679 cumulus convection in the Canadian Climate Centre general circulation model, *Atmosphere-*
680 *ocean*, 33, 407-446, 1995.

681 Zhang, J., Reid, J. S., Westphal, D. L., Baker, N. L., and Hyer, E. J.: A system for operational
682 aerosol optical depth data assimilation over global oceans, *Journal of Geophysical Research:*
683 *Atmospheres*, 113, 2008.

684 Zhang, K., Wan, H., Liu, X., Ghan, S. J., Kooperman, G., Ma, P.-L., Rasch, P. J., Neubauer, D.,
685 and Lohmann, U.: Technical Note: On the use of nudging for aerosol–climate model
686 intercomparison studies, *Atmospheric Chemistry and Physics*, 14, 8631-8645, 2014.

687 Zhang, Z., Meyer, K., Yu, H., Platnick, S., Colarco, P., Liu, Z., and Oreopoulos, L.: Shortwave
688 direct radiative effects of above-cloud aerosols over global oceans derived from 8 years of
689 CALIOP and MODIS observations, *Atmospheric Chemistry and Physics*, 16, 2877-2900, 2016.

690

691



Table 1. List of CAM5 simulations.

Name	Fire emission	Simulation period	Member	Nudging
Group A: Single member simulations				
S_NF	No			
S_GF3	GFED v3			
S_GF4	GFED v4.1	January 1- April 30, 2009	1	Horizontal winds (6h)
S_QF	QFED v2.4			
Group B: Ensemble simulations				
E_NF	No			
E_GF3	GFED v3			
E_GF4	GFED v4.1	April 1 - April 10, 2009	10	Horizontal winds (6h) and temperature (~10d)*
E_QF	QFED v2.4			

* See section 2.3 for details about ensembles

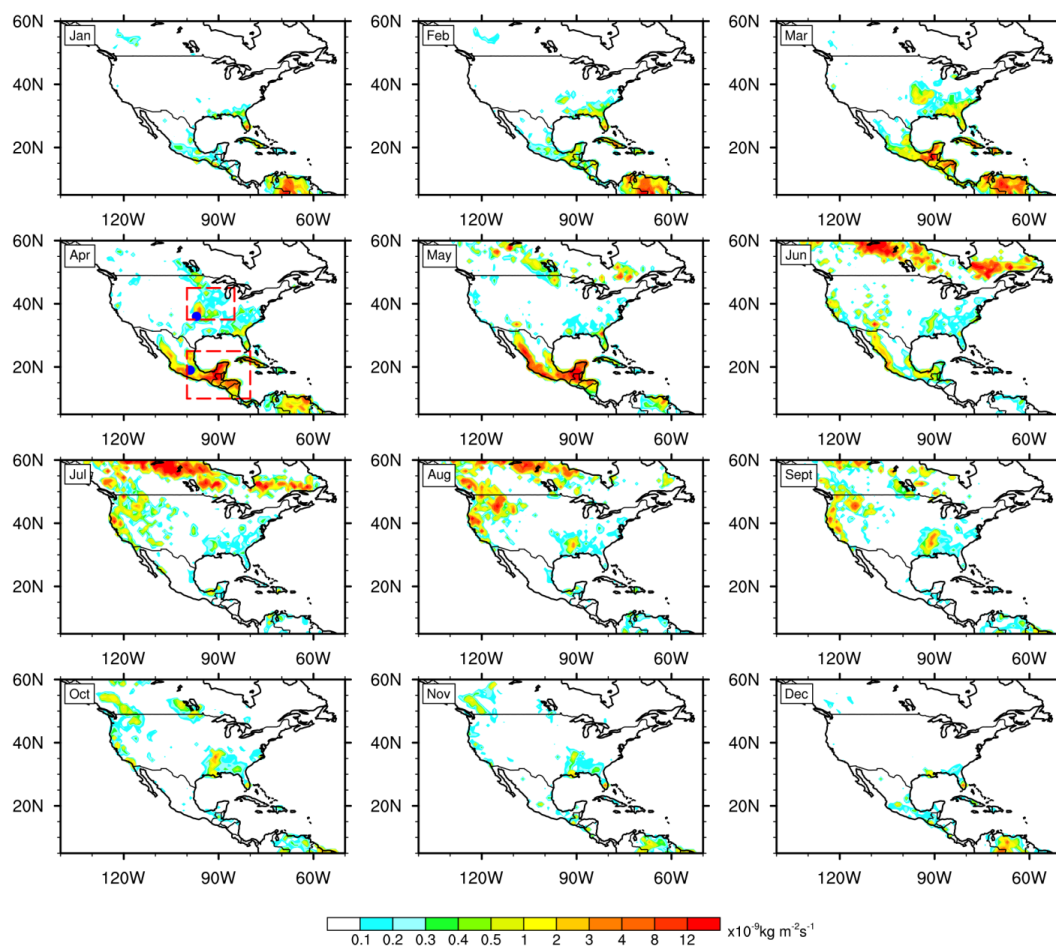


Figure 1. Spatial distributions of multi-year monthly mean biomass burning consumed dry matter over North America during 2003-2014 from GFEDv4.1. Boxes denote selected regions: central U.S (35 - 45°N, 85 - 100°W) and Southern Mexico (10 - 25°N, 80 - 100°W). Dots denote locations of AERONET sites: Cart Site (36°N, 97°W) and Mexico City (19°N, 99°W)

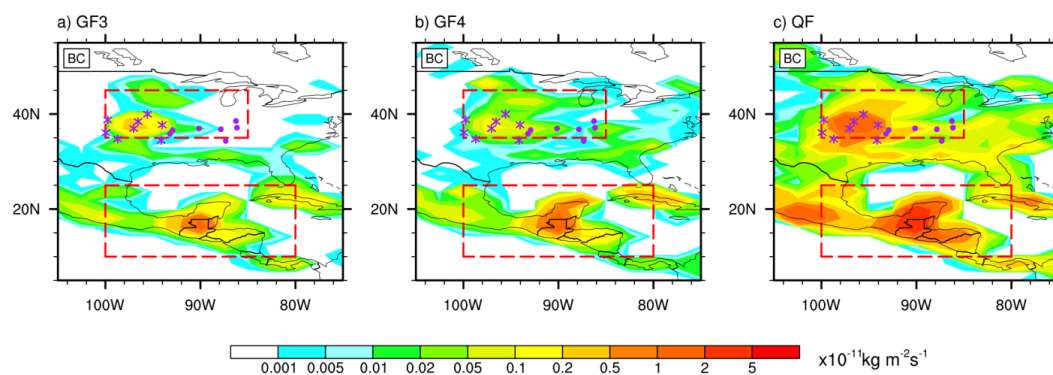


Figure 2. Spatial distributions of monthly mean BC emissions from three emission inventories in April, 2009. IMPROVE data sites are shown as asterisks for sites near the source region and as dots for sites in the region downwind of the fire source.

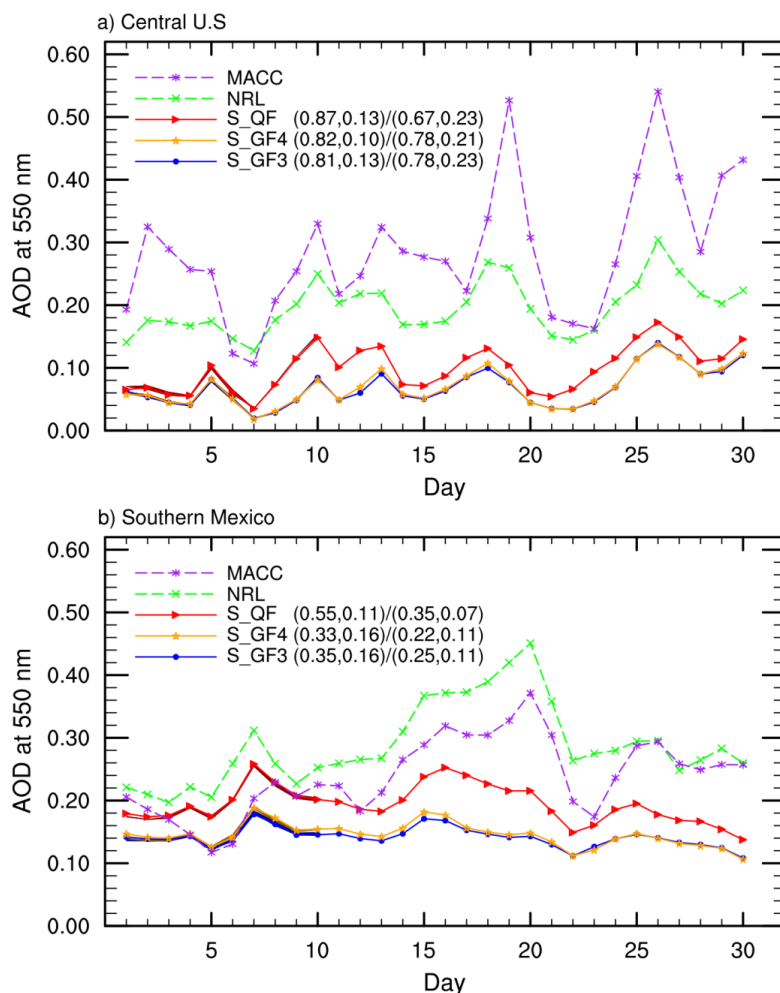


Figure 3. Time series of daily regional mean AOD in April, 2009 in simulations and reanalysis data. Numbers in parenthesis denote TCC and RMSE between each simulation in group A and reanalysis data (left: NRL; right: MACC). Individual lines indicate group A simulations. Shaded areas (very narrow) in slightly darker colors during April 1-10 illustrate maximum and minimum values of daily mean AOD among ensemble members in group B simulations.

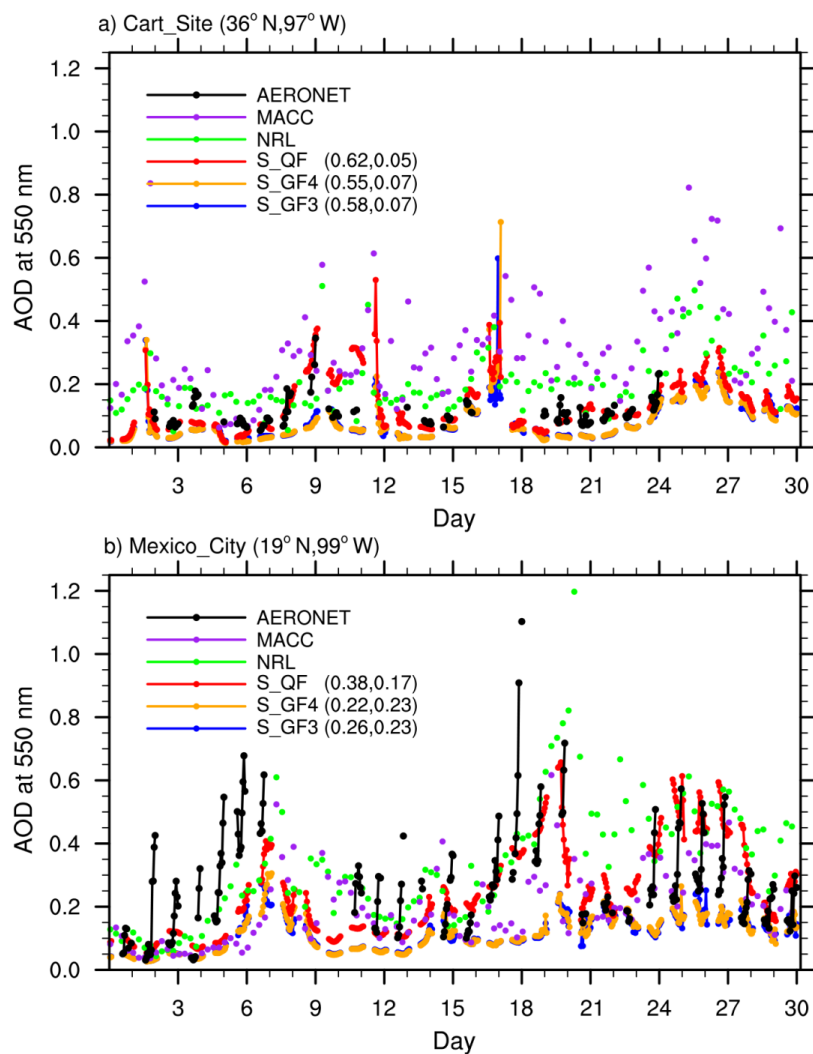


Figure 4. Time series of hourly regional mean AOD in April, 2009 from group A simulations, reanalysis data and AERONET retrievals at AERONET sites. Numbers in parenthesis denote TCC (left) and RMSE (right) between each simulation and AERONET AOD.

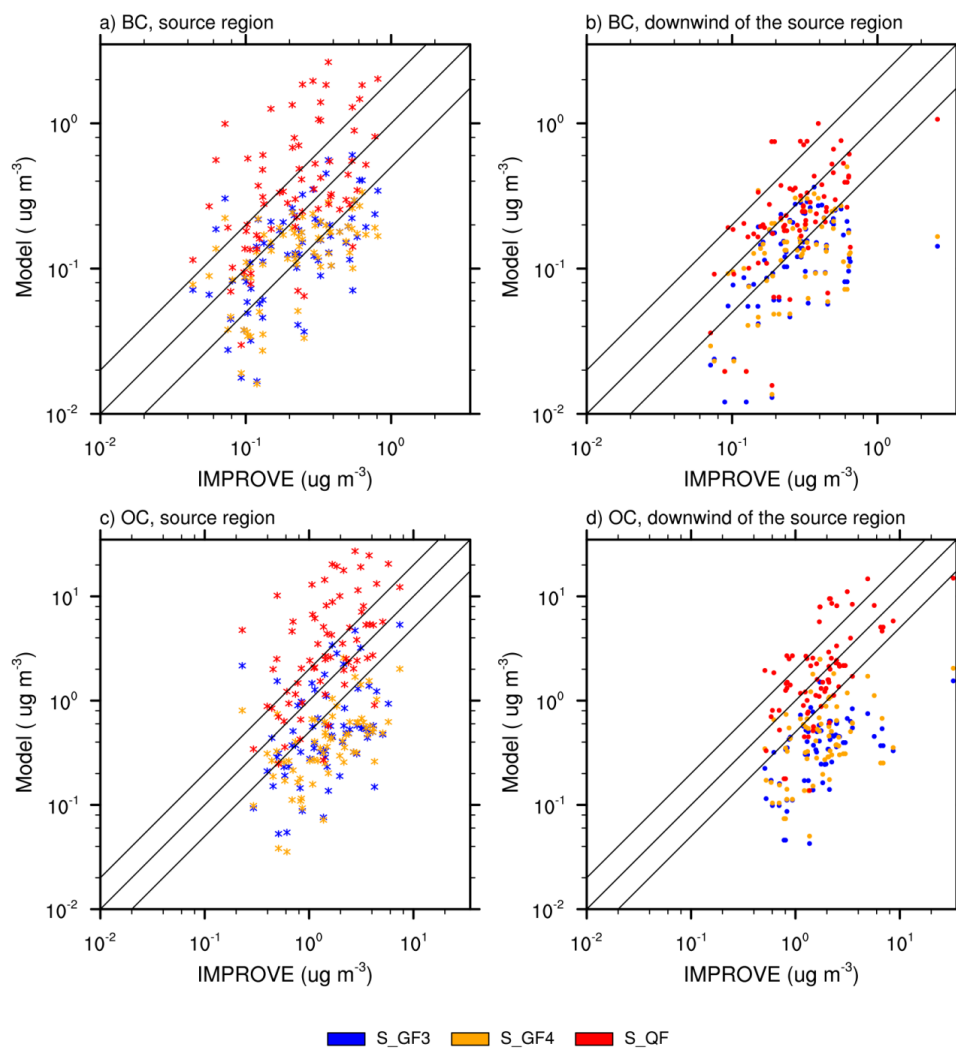


Figure 5. Evaluation of the simulated BC (up) and POM (bottom) concentrations in group A simulations against the IMPROVE data at sites near the source and downwind the source region. Locations of these sites are marked with the same symbol as in Fig. 2.

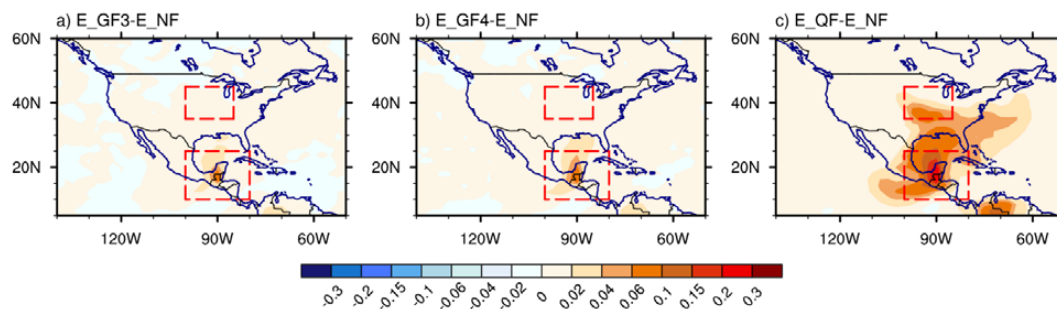


Figure 6. Spatial distributions of 10-day average (Apr. 1-10) ensemble mean AOD differences between simulations with (E_GF3, E_GF4, and E_QF) and without fire emission (E_NF).

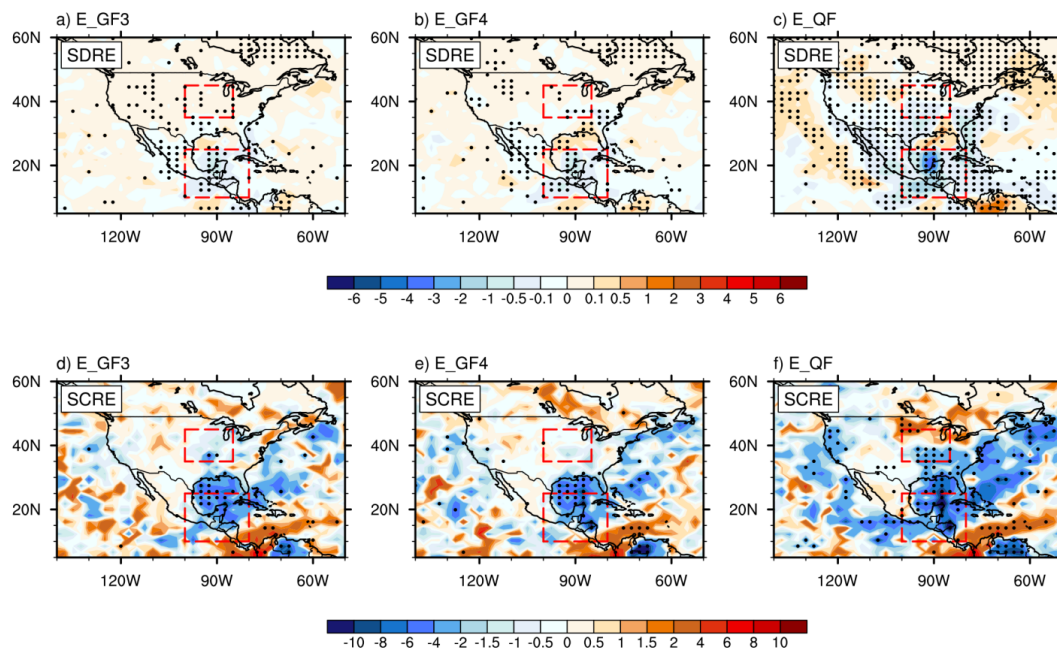


Figure 7. Spatial distributions of 10-day average (Apr. 1-10) ensemble mean fire aerosol shortwave direct radiative effect (SDRE) and shortwave cloud radiative effect (SCRE) ($W m^{-2}$) in group B simulations. Dots denote regions where SDRE is statistically significant at the 95% confidence level based on the KS test.

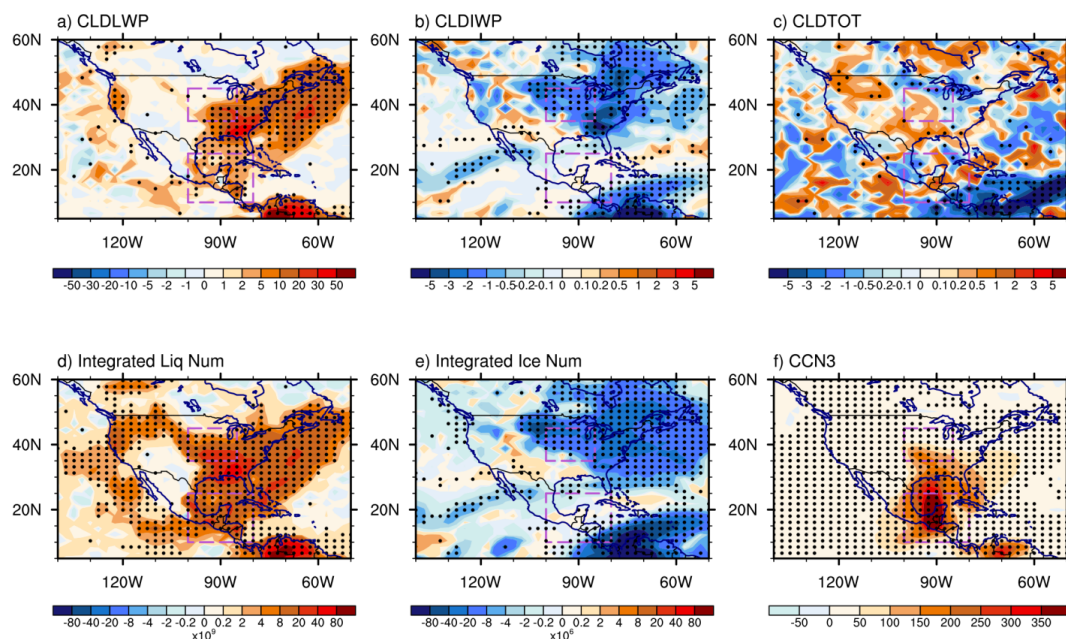


Figure 8. Difference of 10-day average (Apr.1-10) ensemble mean between simulations E_NF and E_QF: a) cloud liquid water path (g m^{-2}), b) cloud ice water path (g m^{-2}), c) total cloud fraction (%), d) column-integrated droplet number concentration (m^{-2}), e) column-integrated ice number concentration (m^{-2}), and f) cloud condensation nuclei at 0.1% supersaturation near 900 hPa. Dots denote regions where the difference is statistically significant at the 95% confidence level based on the KS test.

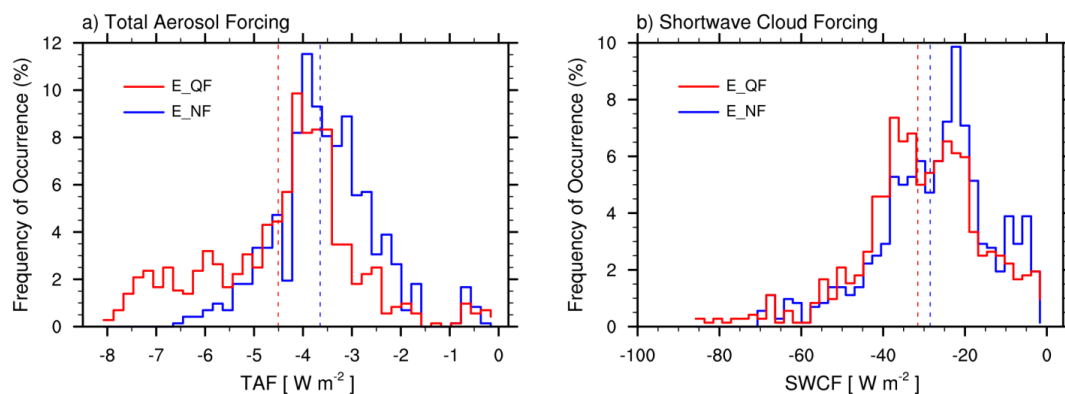


Figure 9. Probability distributions of 10-day average (Apr.1-10) a) total aerosol forcing and b) cloud forcing over Southern Mexico in simulations E_NF and E_QF sampled from grid values of ensemble members (72x10 for each case). Dashed lines indicate the mean of the distribution.

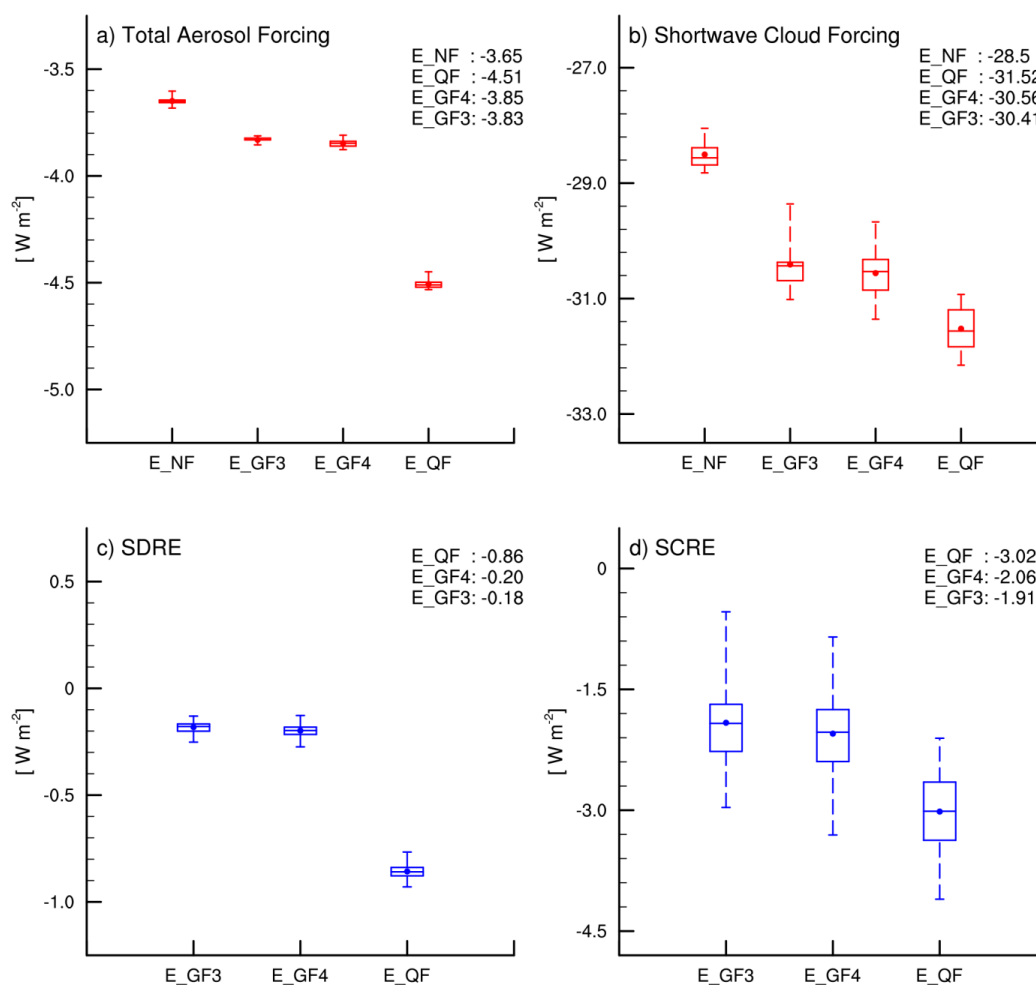


Figure 10. 10-day average (Apr. 1-10) regional mean a) total aerosol forcing, b) total shortwave cloud forcing and fire aerosol, c) SDRE, and d) SCRE in Southern Mexico in group B simulations. Box denotes the 25th and 75th percentiles. Bars outside the box indicate minimum and maximum. Bar within the box denotes the 50th percentile. Total aerosol and cloud forcing are sampled from different ensemble members (10 for each case). Fire aerosol SDRE and SCRF are sampled by calculating the difference between members in simulations E_QF (E_GF3/E_GF4) and E_NF (10x10 for each case).

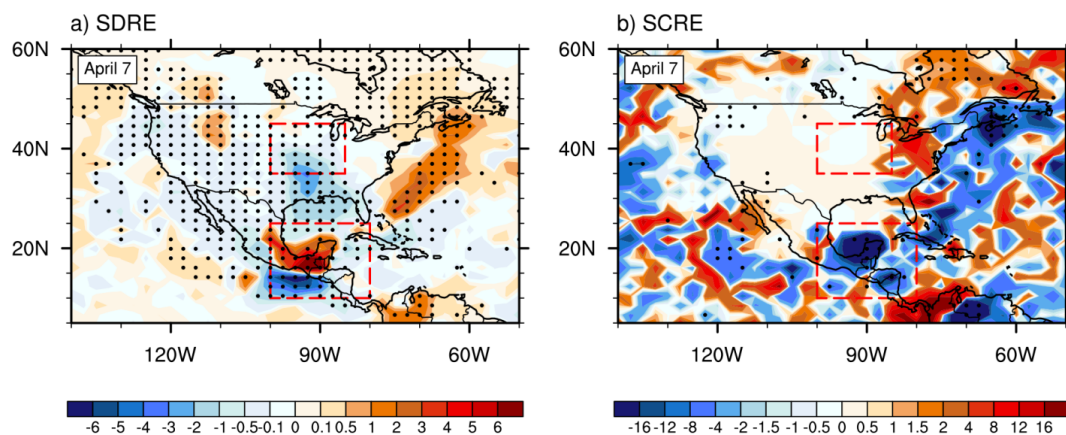


Figure 11. Spatial distributions of ensemble mean fire aerosol a) SDRE and b) SCRE ($W m^{-2}$) on April 7 in the E_QF simulation. Dots denote grids where fire aerosol effect is statistically significant at the 95% confidence level based on the KS test.

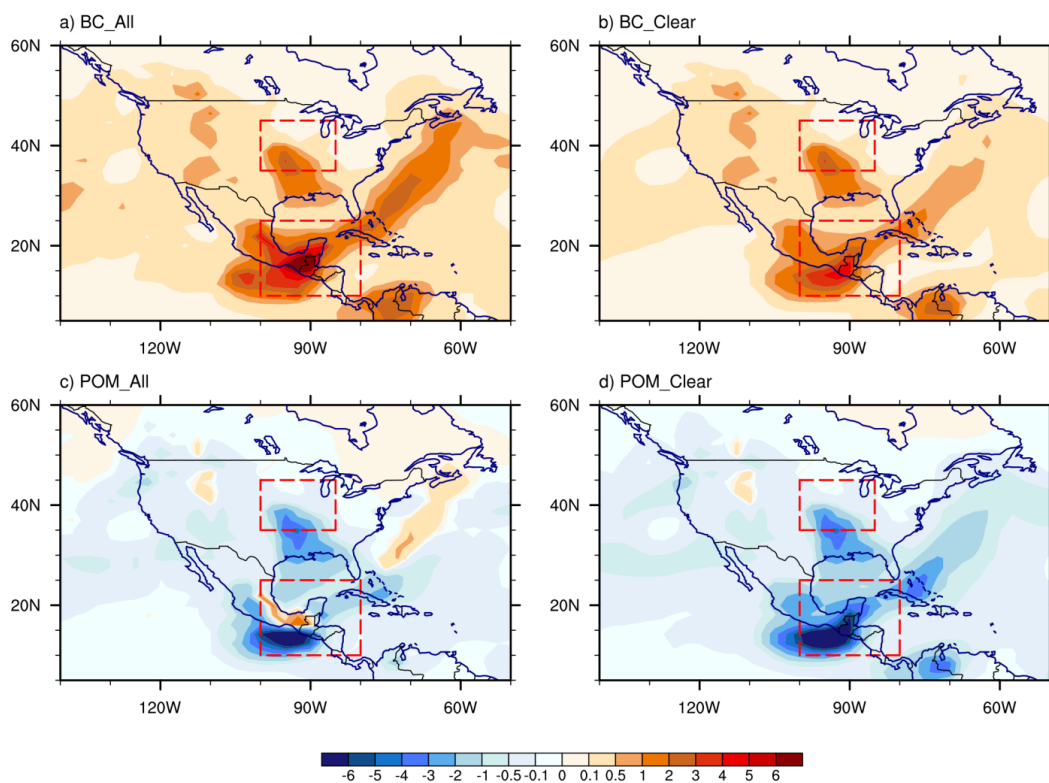


Figure 12. Spatial distributions of fire BC SDRE and fire POM SDRE ($W m^{-2}$) on all-sky and clear-sky conditions on April 7 in the E_QF simulation.

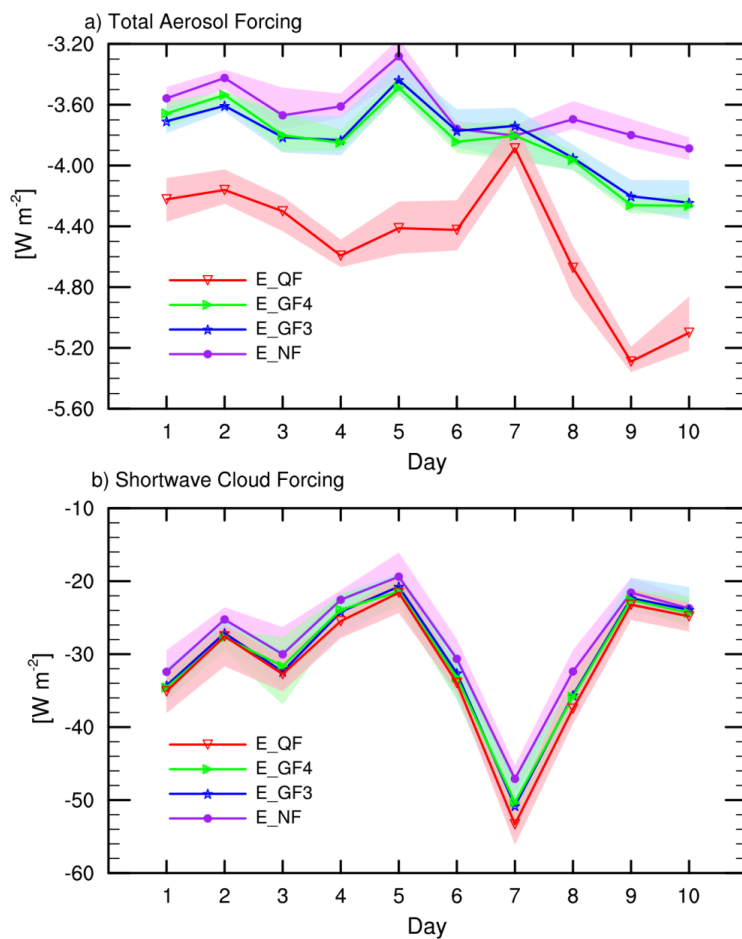


Figure 13. Time series of daily regional mean total a) aerosol forcing and b) cloud forcing in Southern Mexico during Apr. 1-10, 2009 in group B simulations. Individual lines indicate ensemble mean values. Shaded areas illustrate the ensemble spread (from minimum to maximum).

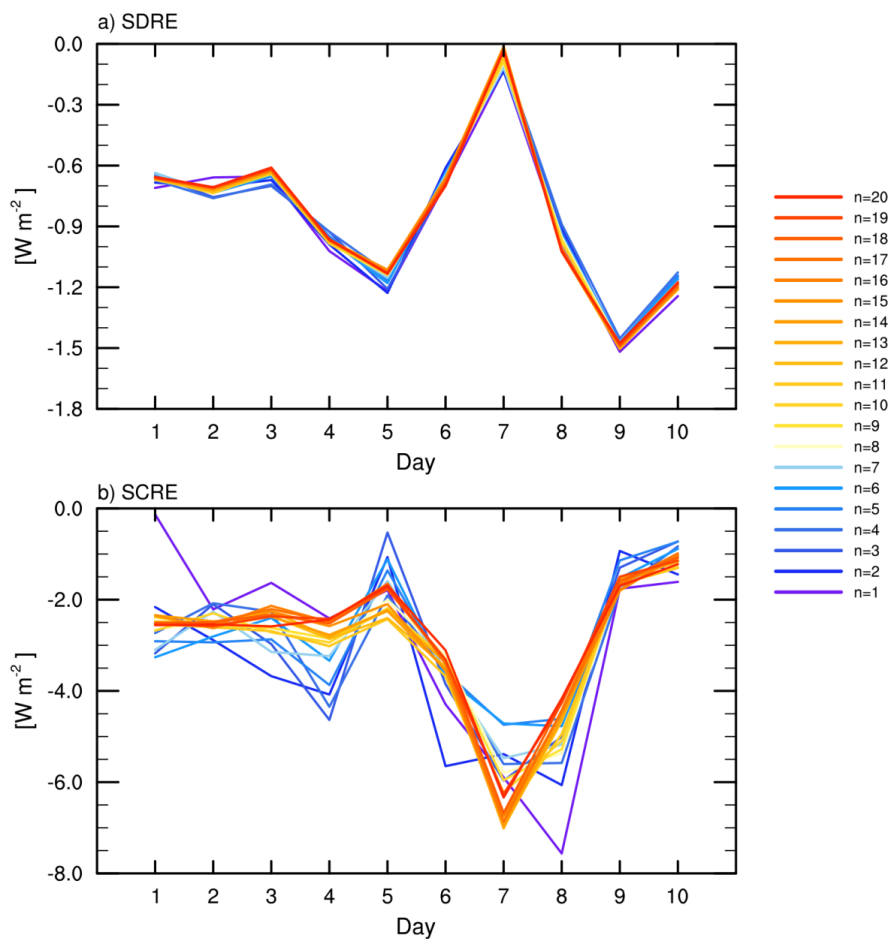


Figure 14. Time series of daily ensemble mean fire aerosol a) SDRE and b) SCRE averaged over Southern Mexico during Apr. 1-10, 2009 in QFED forced ensemble simulations with varying the total number of ensemble members ($n=1-20$).